0022-3565/09/3313-816–826
THE JOURNAL OF PHARMACOLOGY AND EXPERIMENTAL THERAPEUTICS
U.S. Government work not protected by U.S. copyright
JPET 331:816–826, 2009

Vol. 331, No. 3
154997/3533321
Printed in U.S.A.

Cellular Inhibition of Checkpoint Kinase 2 (Chk2) and Potentiation of Camptothecins and Radiation by the Novel Chk2 Inhibitor PV1019 [7-Nitro-1*H*-indole-2-carboxylic acid {4-[1-(guanidinohydrazone)-ethyl]-phenyl}-amide]S

Andrew G. Jobson, George T. Lountos, Philip L. Lorenzi, Jenny Llamas, John Connelly, David Cerna, Joseph E. Tropea, Akikazu Onda, Gabriele Zoppoli, Sudhir Kondapaka, Guangtao Zhang, Natasha J. Caplen, John H. Cardellina II, Stephen S. Yoo, Anne Monks, Christopher Self, David S. Waugh, Robert H. Shoemaker, and Yves Pommier

Laboratory of Molecular Pharmacology (A.G.J., P.L.L., J.L., A.O., G.Zo., Y.P.) and Gene Silencing Section, Genetics Branch (N.J.C.), Center for Cancer Research, National Cancer Institute, National Institutes of Health, Bethesda, Maryland; Macromolecular Crystallography Laboratory (G.T.L., J.E.T., D.S.W.) and Screening Technologies Branch, Developmental Therapeutics Program, Division of Cancer Treatment and Diagnosis (S.K., J.H.C., R.H.S.), National Cancer Institute, National Institutes of Health, Frederick, Maryland; Laboratory of Functional Genomics (J.C., A.M.) and Molecular Radiation Therapeutics Branch (D.C.), SAIC-Frederick, National Cancer Institute-Fredrick, Frederick, Maryland; Provid Pharmaceuticals, North Brunswick, New Jersey (G.Zh., C.S.); and Molecular Radiation Therapeutics Branch, Radiation Research Program, Division of Cancer Treatment and Diagnosis, National Cancer Institute, National Institutes of Health, Rockville, Maryland (S.S.Y.)

Received April 13, 2009; accepted September 3, 2009

ABSTRACT

Chk2 is a checkpoint kinase involved in the ataxia telangiectasia mutated pathway, which is activated by genomic instability and DNA damage, leading to either cell death (apoptosis) or cell cycle arrest. Chk2 provides an unexplored therapeutic target against cancer cells. We recently reported 4,4′-diacetyldiphenylurea-bis(guanylhydrazone) (NSC 109555) as a novel chemotype Chk2 inhibitor. We have now synthesized a derivative of NSC 109555, PV1019 (NSC 744039) [7-nitro-1*H*-indole-2-carboxylic acid {4-[1-(guanidinohydrazone)-ethyl]-phenyl}-amide], which is a selective submicromolar inhibitor of Chk2 in vitro. The cocrystal structure of PV1019 bound in the ATP binding pocket of Chk2 confirmed enzymatic/biochemical observations that PV1019 acts as a competitive inhibitor of Chk2 with respect to ATP. PV1019 was found to inhibit Chk2 in cells. It inhibits Chk2 autophosphorylation (which represents the cellular kinase activation of Chk2), Cdc25C phosphorylation, and HDMX degradation in response to DNA damage. PV1019 also protects normal mouse thymocytes against ionizing radiation-induced apoptosis, and it shows synergistic antiproliferative activity with topotecan, camptothecin, and radiation in human tumor cell lines. We also show that PV1019 and Chk2 small interfering RNAs can exert antiproliferative activity themselves in the cancer cells with high Chk2 expression in the NCI-60 screen. These data indicate that PV1019 is a potent and selective inhibitor of Chk2 with chemotherapeutic and radiosensitization potential.

Chk2 is pivotal in mediating the DNA damage signal after genotoxic stress, leading to either DNA repair or apoptosis, depending on the severity of the damage and the genetic background of the cells. In addition, it has been proposed that Chk2 functions as a barrier to tumorigenesis by maintaining genomic stability because the DNA damage response is activated early in cancer lesions, and this DNA damage induction is thought to prevent or delay genetic instability and tumorigenesis (Bartkova et al., 2005; Gorgoulis et al., 2005).

This work was supported by the Intramural Research Program of the National Institutes of Health National Cancer Institute. X-ray diffraction data were collected at the Southeast Regional Collaborative Access Team (SER-CAT) beamlines 22-ID and 22-BM at the Advanced Photon Source, Argonne National Laboratory. Supporting institutions may be found at http://www.ser-cat.org/members.html. Use of the Advanced Photon Source was supported by the U.S. Department of Energy, Office of Science, Office of Basic Energy Sciences [Contract W-31-109-Eng-38].

Article, publication date, and citation information can be found at http://jpet.aspetjournals.org.

doi:10.1124/jpet.109.154997.

S The online version of this article (available at http://jpet.aspetjournals.org) contains supplemental material.

ABBREVIATIONS: Chk2, checkpoint kinase 2; ATM, ataxia telangiectasia mutated; siRNA, small interfering RNA; HEK, human embryonic kidney; IR, ionizing radiation; NSC 109555, 4,4′-diacetyldiphenylurea-bis(guanylhydrazone); VRX046617, 3-hydroxy-*N*-isopropyl-5-(4-phenoxy-phenylamino)isothiazole-4-carboximidamine; AZD7762, 3-(carbamoylamino)-5-(3-fluorophenyl)-*N*-(3-piperidyl)thiophene-2-carboxamide; DMSO, dimethyl sulfoxide; RNAi, RNA interference; PBS, phosphate-buffered saline; ABI, 2-arylbenzimidazole; TPT, topotecan; CPT, camptothecin.

After DNA damage, Chk2 is activated primarily by ATM and DNA-dependent (DNA-PK) protein kinase via phosphorylation of Thr^{68} on Chk2 (Ahn et al., 2000), which in turn causes homodimerization and subsequent *trans*-activating autophosphorylations of Thr^{383} and Thr^{387} (Ahn and Prives, 2002) and *cis*-phosphorylation of Ser^{516} (Wu and Chen, 2003). After activation, Chk2 phosphorylates a number of downstream substrates involved in various cellular processes, including cell cycle arrest, apoptosis, and DNA repair and mitosis. For a comprehensive overview of these interactions see Pommier et al. (2005, 2006) and http://discover.nci.nih.gov/mim.

There are a number of studies suggesting therapeutic value of Chk2 inhibitors [for review, see Pommier et al. (2005) and Antoni et al. (2007)]. The primary rationale for targeting Chk2 in cancer therapy is combination with genotoxic agents. Antisense inhibition of Chk2 increased apoptosis in p53-defective HEK293 cells (Yu et al., 2001). Down-regulation of Chk2 augmented the effect of paclitaxel in MCF7 cells (Chabalier-Taste et al., 2008). Chk2 inhibition also enhanced the level of mitotic catastrophe when used in combination with either doxorubicin (Castedo et al., 2004) or cisplatin (Vakifahmetoglu et al., 2008). In addition, Chk2 siRNA down-regulation or a dominant-negative form of Chk2 prevented the release of the antiapoptotic factor survivin from the mitochondria, thus augmenting ionizing radiation (IR)- or doxorubicin-induced apoptosis (Ghosh et al., 2006). Furthermore, doxycycline-induced expression of the dominant-negative form of Chk2 potentiated the cytotoxic effect of doxorubicin in HCT116 xenografts in mice. In addition to augmenting the effect of cytotoxic drugs, Chk2 inhibitors may elicit radio- or chemoprotection of normal tissue via abrogation of p53-dependent apoptosis (Pommier et al., 2005; Antoni et al., 2007). In support of this finding, Chk2-null mice are viable but show increased survival when exposed to ionizing radiation (Hirao et al., 2000; Takai et al., 2002). That effect has also been demonstrated using Chk2 inhibitors in either mouse thymocytes (Carlessi et al., 2007) or isolated $CD4^+$ and $CD8^+$ human lymphocytes (Arienti et al., 2005).

An additional rationale for the therapeutic development of Chk2 inhibitors is the increased levels of activated Chk2 in some human tumor cells. It is plausible that cells in which Chk2 is constitutively activated have adapted and become addicted to Chk2 to survive. In that situation, inhibition of Chk2 may cause cell death. Activated Chk2 has also been found to be important in viral replication. In particular, down-regulation of Chk2 by short hairpin RNA in cells infected with hepatitis C led to abrogation of viral replication (Ariumi et al., 2008). Furthermore, the ATM-mediated DNA damage response pathway has been implicated in human immunodeficiency virus replication (Lau et al., 2005). Small molecule inhibition of ATM caused a decrease in human immunodeficiency virus replication, again suggesting a role for the ATM-Chk2 pathway in virus replication and a benefit for antivirus therapy with a Chk2 inhibitor.

Only a few selective Chk2 inhibitors have been reported: NSC 109555 (Jobson et al., 2007), 2-arylbenzimidazole (Arienti et al., 2005), VRX0466617 (Carlessi et al., 2007), and a series of isothiazole carboxamides (Larson et al., 2007), and none is known to be under clinical development. However, many more dual Chk1/Chk2 inhibitors are known, e.g., debromohymenialdisine (Curman et al., 2001), debromohymenialdisine analog (Sharma and Tepe, 2004), the aminopyrazine derivative XL-844 (Matthews et al., 2007), the thiophene urea carboxamide AZD7762 (Zabludoff et al., 2008), and the diazepinoindolone PF-473336 (Ashwell et al., 2008), with the final three compounds currently undergoing early clinical evaluation. Of these three compounds, AZD7762 is approximately equipotent against Chk1 and Chk2, whereas PF-477736 and XL-844 are more selective against Chk1 than against Chk2 (Lapenna and Giordano, 2009). The occurrence of dual Chk1/Chk2 inhibitors is not unexpected given that Chk1 and Chk2 are part of the Ca^{2+}/calmodulin-dependent protein kinase family in the kinome (Manning et al., 2002). Recent insights into the cocrystal structures of Chk2 inhibitors bound in the ATP-binding pocket of Chk2 will enable improved, selective drug design. Here we present both in vitro and cellular data showing selective inhibition of Chk2 in biochemical and cellular assays and potentiation of cytotoxic agents and radiation by a novel Chk2 inhibitor PV1019.

Materials and Methods

Expression and Purification of Recombinant Proteins. The expression and purification of recombinant Chk2 and Cdc25C have been described in detail elsewhere (Yu et al., 2002; Jobson et al., 2007). Recombinant Chk1 was purchased from Millipore (Billerica, MA). Histone H1, from calf thymus, was purchased from Roche Diagnostics (Indianapolis, IN).

Protein Kinase Assays. In vitro protein kinase assays were performed as described previously with minor modifications (Jobson et al., 2007). Drugs were dissolved in DMSO, in which case the final DMSO concentration in assays was 1% and the control assays were performed under comparable conditions. Chk2 protein kinase activity, measured as ^{32}P incorporation into Chk2, GST-Cdc25C, or histone H1, was determined using a PhosphorImager (GE Healthcare, Little Chalfont, Buckinghamshire, UK). Densitometry was performed using ImageQuant (GE Healthcare). For competitive inhibition studies Chk2 was incubated with GST-Cdc25C for 10 min at 30°C. The ratio of "cold" ATP and ^{32}P-labeled γ-ATP was kept constant while the concentration was altered (100, 50, 40, and 25 μM). This set of reactions was repeated in the presence of 0.25, 0.5, and 0.75 μM PV1019.

Cell Culture, RNAi, and Cell Viability Assay. MCF7 cells were grown in DMEM with L-glutamine, supplemented with 10% fetal calf serum. OVCAR-3, OVCAR-4, and OVCAR-5 cell lines were maintained in RPMI 1640 medium (Lonza Walkersville, Inc., Walkersville, MD) containing 5% fetal bovine serum, 2 mM L-glutamine, and no antibiotics. MCF7, OVCAR-4, OVCAR-5, and OVCAR-8 cell lines were tested for *Mycoplasma* using the MycoAlert assay (Lonza Walkersville, Inc.) at the commencement of this study and found to be negative. Mouse thymocytes were isolated from wild-type or *Chk2*(−/−) mice by mechanical disaggregation and grown in DMEM with L-glutamine, supplemented with 15% fetal calf serum.

For RNAi-mediated gene silencing, OVCAR-4 and OVCAR-8 cells were seeded with a complex of either negative siRNA (AllStars Negative; QIAGEN, Valencia, CA) or a previously validated *CHEK2* siRNA (target sequence 5′ACGCCGTCCTTTGAATAACAA 3′) (Zhang et al., 2009) and Oligofectamine (Invitrogen, Carlsbad, CA) at a range of concentrations (Fig. 6, C and D). After 48 h of incubation, the siRNA/lipid complex-containing medium was replaced by fresh medium. After a further 48 h of incubation, cells were assayed for cell viability using a standard MTS assay ($A_{490\ nm}$) (Promega, Madison, WI).

Western Blot Analyses and Antibodies. Whole-cell lysates were prepared as described previously (Solier et al., 2009), and nuclear extract samples were prepared using a nuclear extract kit, following the manufacturer's instructions (Active Motif Inc., Carlsbad, CA). Samples were subjected to SDS-polyacrylamide gel electrophoresis, and the gels were transferred to polyvinylidene difluo-

ride membranes. The membranes were blocked with either 5% milk (Tris-buffered saline/Tween 20) or 5% bovine serum albumin (Tris-buffered saline/Tween 20), incubated overnight at 4°C with primary antibodies, washed, and then incubated for 1 h with secondary antibodies [peroxidase-conjugated goat anti-mouse IgG or peroxidase-conjugated goat anti-rabbit IgG (GE Healthcare)]. Signals were revealed by autoradiography using an Enhanced Chemiluminescence Detection Kit (Pierce Chemical, Rockford, IL).

The following primary antibodies were used: anti-P-Chk2 Ser^{516} (Cell Signaling Technology Inc., Danvers, MA), anti-Chk2 (Cell Signaling Technology Inc,), anti-HDMX Bethyl Laboratories, Montgomery, TX), and anti-P-Cdc25C Ser^{216} (Cell Signaling Technology Inc.).

Sub-G_1 Analysis of Mouse Thymocytes by Flow Cytometry. Three million cells were exposed to 5 Gy of IR or control in the presence or absence of 1 μM PV1019. The cells were further incubated at 37°C for 16 h before fixation and permeabilization with cold (−20°C) 70% ethanol overnight and washed with PBS. Propidium iodide (final concentration 0.05 mg/ml) and RNase A (final concentration 0.5 mg/ml) were added. Fluorescence intensities were determined using a FACScan flow cytometer (BD, Franklin Lakes, NJ) and quantified using CellQuest software (BD). Data were analyzed by FlowJo software (TreeStar Inc., Ashland, OR).

Drug Treatment and Synergy. For drug concentration-effect experiments, cells were seeded at appropriate densities (to yield ~80% confluence at time of assay) in 96-well plates and incubated at 37°C for 48 h before drug addition. At 48 h, serial dilutions of each drug (10 mM stock in DMSO) were prepared in medium. After medium was aspirated from cells, 100 μl of drug solution was added to appropriate wells. The plates were incubated at 37°C for 48 h. Cell proliferation was assayed by adding 20 μl of 3-(4,5-dimethylthiazol-2-yl)-5-(3 carboxymethoxyphenyl)-2-(4-sulfophenyl)-2*H*-tetrazolium (MTS) (Promega) to each well, incubating at 37°C for 1 h and then reading plates at 490 nm. The data were plotted using GraphPad Prism (GraphPad Software Inc., San Diego, CA) from raw absorbance values and were not normalized to the control. The effect of single drugs alone is depicted at zero on the *x*-axis. Combination indices were calculated using CalcuSyn software (Biosoft, Cambridge, UK).

Clonogenic Survival Assays. The human glioma cell line U251 (American Type Culture Collection, Manassas, VA) was grown in RPMI 1640 medium containing glutamate (5 mM) and 5% fetal bovine serum at 37°C in 5% CO_2 and 95% room air. A specific number of U251 cells were plated into each well of the six-well culture plates. After cells were allowed to attach for 16 h, they were treated with PV1019 (5 μmol/l) or DMSO (vehicle control) for 1 h and then irradiated with a Pantak X-ray source at a dose rate of 2.28 Gy/min. Two hours after irradiation cells were rinsed with PBS and were placed in fresh growth medium. The cells were further incubated for colony formation for 10 days. Colonies were fixed with methanol and stained with 0.5% crystal violet. The number of colonies containing at least 50 cells was determined, and surviving fractions were calculated. Each data point was determined in triplicate. Radiation survival data were fitted to a linear-quadratic model using KaleidaGraph (version 4.0; Synergy Software, Reading, PA) after normalizing for cell killing by PV1019 alone. Each point on the survival curves represents the mean surviving fraction ± S.E. from four independent experiments.

Kinase Profiling. Kinase profiling was performed using HotSpot technology (Reaction Biology Corp., Malvern, PA). This technology is a radioisotope-based P81 filter-binding assay. PV1019 was dissolved in pure DMSO to make a 10 mM stock. PV1019 was then diluted in pure DMSO to make a serial dilution based on the IC_{50} ranges. Chk2 and substrate [20 μM CHKtide (KKKVSRSGLYRSPSMPENLNRPR)] were diluted in the reaction buffer (20 mM HEPES, pH 7.5, 10 mM $MgCl_2$, 1 mM EGTA, 0.02% Brij 35, 0.02 mg/ml bovine serum albumin, 1 mM Na_3VO_4, 2 mM dithiothreitol, and 1% DMSO), and then 5 nl of compound was delivered into Chk2 and substrate mixture by acoustic technology using Echo 550 (LabCyte Inc., Sunnyvale, CA). The reaction was initiated by the addition of [^{33}P]ATP into the reaction mixture (final concentration was 10 μM) and stopped after 2 h of incubation at room temperature. The unreacted free [^{33}P]ATP was washed away before detection.

Results

Biochemical Characterization of PV1019 (NSC 744039). We recently reported the identification of a novel and specific Chk2 inhibitor, NSC 109555 (Jobson et al., 2007) (Fig. 1A). However, NSC 109555 did not show detectable Chk2 inhibition in a cellular environment. For this reason we sought to optimize the molecule. Figure 1A shows the structure of PV1019—an analog of NSC 109555 we designed from the crystal structure (Lountos et al., 2009) and selected for the present study. As part of the optimization process we desymmetrized the lead molecule (NSC 109555), retaining one of the guanidinohydrazone moieties and coupling this via an amide bond to a 7-nitroindole substituent (shown as dotted box for PV1019) (Supplemental Materials and Methods). An in vitro kinase assay was used to demonstrate inhibition of Chk2 function by PV1019 (NSC 744039) (Jobson et al., 2007). Figure 1B shows the dose-dependent inhibition of both Chk2 autophosphorylation and histone H1 phosphorylation. The IC_{50} for PV1019 was 138 nM, which demonstrates that PV1019 is slightly more potent than the parent compound NSC 109555 (240 nM) (Jobson et al., 2007). We also assessed whether PV1019 could inhibit Chk2-mediated phosphorylation of Cdc25C, which is a known substrate of Chk2 in vivo (Matsuoka et al., 1998). As Fig. 1C shows, PV1019 inhibits the Chk2-dependent phosphorylation of Cdc25C in a dose-dependent fashion with an IC_{50} of 260 nM. The specificity of PV1019 for Chk2 over Chk1 was investigated and is shown in Fig. 1C. The IC_{50} for PV1019-mediated inhibition of Chk1 autophosphorylation was 55 μM, indicating the specificity of PV1019 for Chk2 over Chk1.

To further characterize the mechanism of action of PV1019, we assessed whether PV1019 acted as a competitive inhibitor of Chk2 with respect to ATP (Fig. 1D). Lineweaver-Burk analysis showed that, like the parent compound NSC 109555, PV1019 is a competitive ATP inhibitor for Chk2. Given the physiological concentration of ATP in a cellular environment, we sought to determine the impact of physiological ATP concentrations on the efficacy of PV1019. In vitro kinase assays were performed using 1 mM ATP. Figure 1E shows that the IC_{50} of PV1019 was 0.57 μM under these conditions, which is 4-fold higher than the IC_{50} determined at 10 μM ATP (Fig. 1B).

Cocrystal Structure of the Catalytic Domain of Chk2 in Complex with PV1019. To elucidate the binding mode of PV1019 to Chk2, we cocrystallized the catalytic domain (residues 210–534) with the inhibitor (Supplemental Materials and Methods). The structure was refined to 2.07 Å resolution (Supplemental Table 1). The electron density maps are clearly resolved (Fig. 2A) and reveal that PV1019 is located in the ATP-binding pocket of Chk2 (Fig. 2B), as expected, because it is a competitive inhibitor of ATP binding (Fig. 1D). Overall, the cocrystal structure is very similar to that of Chk2 in complex with ADP (root mean S.D. = 0.47 Å) and does not exhibit any significant conformational changes (Oliver et al., 2006). Electrospray mass spectrometry indicates that the purified Chk2 is phosphorylated and is thus in an

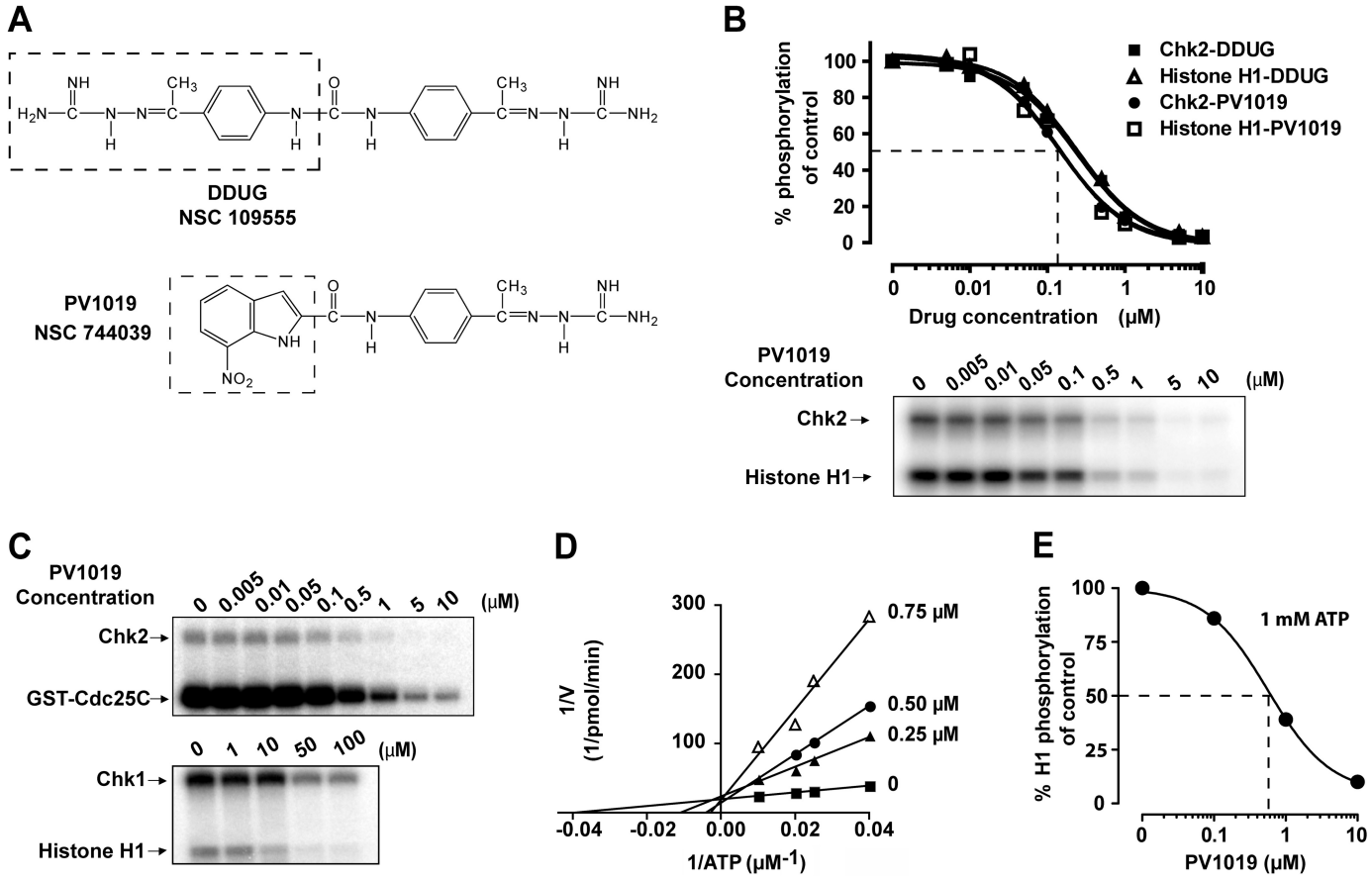

Fig. 1. PV1019 is a selective and potent inhibitor of Chk2 in vitro. A, structures of NSC 109555 (Jobson et al., 2007) and PV1019. The differences are shown by dotted boxes. B, Chk2 was incubated with histone H1 and various concentrations of either NSC 109555 or PV1019 for the indicated times in an in vitro kinase assay. A representative gel of a Chk2 inhibitor experiment for PV1019 is shown. C, effect of increasing concentrations of PV1019 on Chk2 and GST-Cdc25C (top) and on Chk1 and histone H1 phosphorylation (bottom). Representative gels are shown. D, competitive inhibition of Chk2 by PV1019 with respect to ATP. The data are plotted using double reciprocal (Lineweaver-Burk) plots. E, effect of 1 mM ATP on PV1019-mediated inhibition of Chk2. Chk2 was incubated with histone H1 and various concentrations of PV1019 in an in vitro kinase assay containing 1 mM ATP. The percentage inhibition of Chk2-mediated histone H1 phosphorylation is represented graphically.

active conformation (data not shown). The binding of PV1019 to Chk2 is facilitated by hydrogen bonds between the guanidinium terminus of the ligand and Glu^{273} on the C-α helix and the oxygen of the 7-nitroindole of PV1019 to the backbone amide of Met^{304} in the hinge region (Fig. 2C). There are also two important stabilizing water-mediated hydrogen bonds between the carbonyl oxygen and the oxygen of the 7-nitro group on the ligand to the backbone carbonyl of Glu^{302} in the hinge and an additional water-mediated hydrogen bond between the amide nitrogen of PV1019 and the side chain carboxyl oxygen of Glu^{308}. In addition, several van der Waals interactions between the ATP-binding pocket and PV1019 create highly complementary surfaces. The aryl and methyl moieties of the PV1019 phenyl guanidinohydrazone are involved in hydrophobic interactions with Val^{234}, Ile^{251}, Leu^{354}, Ile^{299}, and the aliphatic portions of the side chains of Lys^{249}, Thr^{367}, and Asp^{368}. The 7-nitroindole substituent on the ligand is also involved in hydrophobic interactions with Leu^{226}, Leu^{303}, Gly^{307}, Leu^{354}, and the aliphatic portions of the side chains of Met^{304} and Glu^{308}.

Kinase Profiling of PV1019. To determine the selectivity of PV1019 for Chk2, in vitro kinase-profiling experiments were performed. The inhibitory activity of PV1019 over a panel of 53 cellular kinases indicates that PV1019 is selective toward Chk2 (Table 1). Only 13 other kinases (shown in bold text) showed some inhibition by PV1019, but their IC_{50} values were at least 75-fold greater than those for Chk2. Consistent with the prior results shown in Fig. 1C, PV1019 did not inhibit Chk1. These data demonstrate the specificity of PV1019 for Chk2.

Cellular Inhibition of Chk2 by PV1019. To look for evidence of cellular inhibition of Chk2 by PV1019, we focused on three known substrates of Chk2: Chk2 itself (autophosphorylation), HDMX, and Cdc25C. An abbreviated molecular interaction map of these phosphorylations is depicted in Fig. 3A. The dose-dependent effect of PV1019 on IR-induced Chk2 autophosphorylation at Ser^{516} in OVCAR-4 cells is shown in Fig. 3B. The IC_{50} was 5 μM. Total Chk2 levels were also measured in these experiments, and at lower concentrations of PV1019 showing inhibition of Chk2 autophosphorylation, there was no change in the level of Chk2. It is interesting to note that at higher concentrations of PV1019, there was a decrease in the level of Chk2 total protein. In addition, we assessed the degree of Chk2 inhibition using a previously reported Chk2 inhibitor, 2-arylbenzimidazole (ABI) (Fig. 3C). ABI showed a comparable level of Chk2 inhibition at 25 μM compared with that seen with PV1019. To further investigate the effect of PV1019 on Chk2 inhibition, we used OVCAR-5 cells (which were used for synergy studies later). We assessed two different protocols for topotecan (TPT) and PV1019 ex-

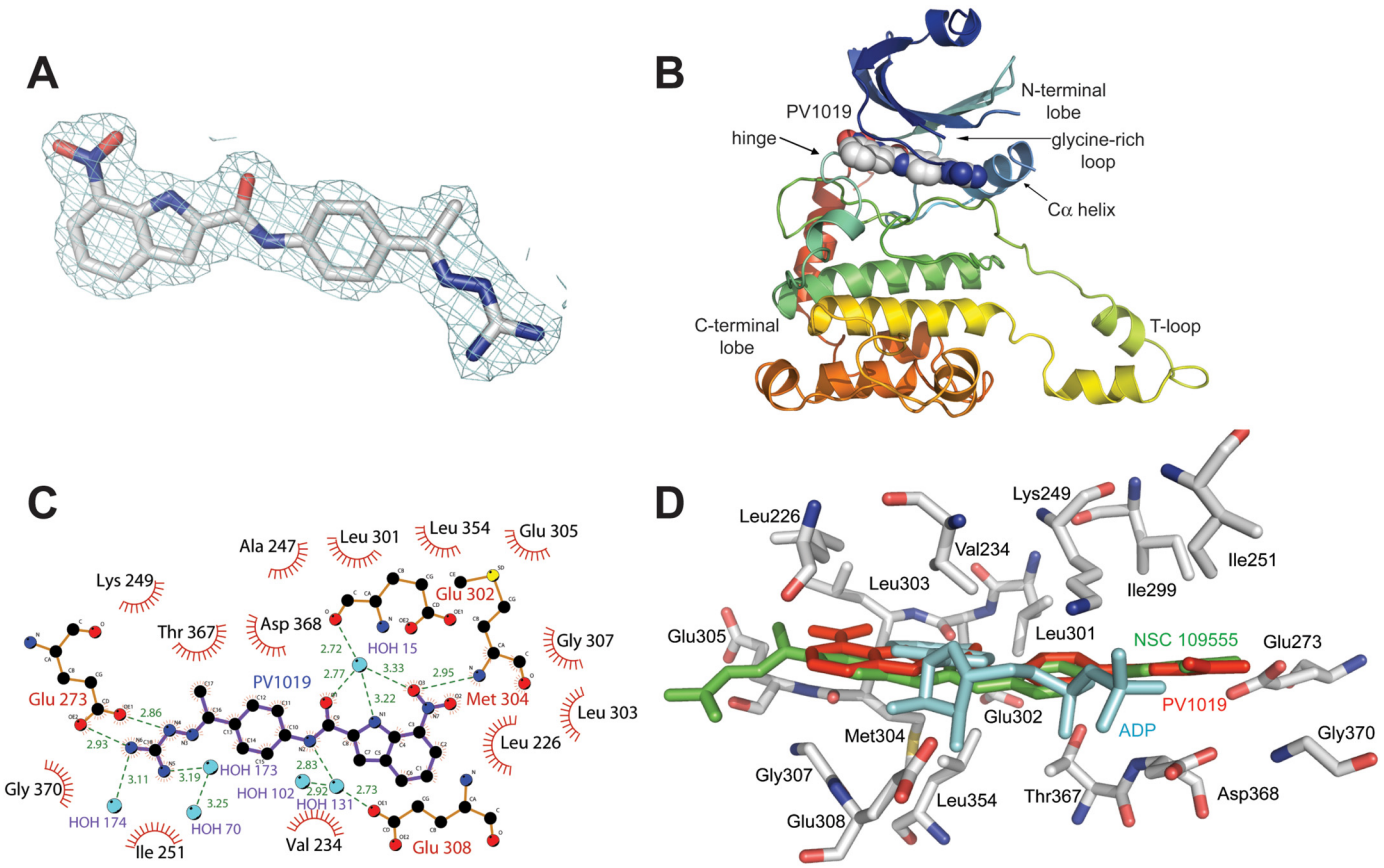

Fig. 2. Cocrystal structure of PV1019 bound in the ATP-binding pocket of the catalytic domain of Chk2. A, coordinates of PV1019 superimposed on the final $2F_o - F_c$ electron density maps at 2.07 Å resolution contoured at the 1σ level. Atoms are colored as carbon (gray), nitrogen (blue), and oxygen (red). B, crystal structure of the catalytic domain of Chk2 in complex with PV1019. The protein is illustrated in ribbons, and the inhibitor is shown in space-filling spheres with carbon (gray), nitrogen (blue), and oxygen (red). C, LIGPLOT schematic diagram of the molecular interactions of PV1019 with the ATP-binding pocket of Chk2. Residues involved in hydrogen bonding to the ligand are illustrated in stick format, water molecules are shown as cyan spheres, and hydrogen bonds are shown as green dashes. The "half-suns" represent hydrophobic interactions between the protein and ligand. D, superposition of the Chk2-PV1019 [red sticks, Protein Data Bank (PDB) code: 2w7x] complex with Chk2-NSC 109555 (green sticks, PDB code: 2w0j), and Chk2-ADP (cyan sticks, PDB code: 2cn5) complexes illustrating the binding conformations of the two inhibitors and ADP. The protein side chain coordinates are from the Chk2-PV1019 structure with carbon (gray), nitrogen (blue), oxygen (red), and sulfur (yellow).

posure, coincubation (Fig. 3C) and pretreatment with TPT, followed by PV1019 treatment (Fig. 3D). The level of Chk2 autophosphorylation (Ser^{516}) was measured by Western blotting. In both cases PV1019 was shown to inhibit the TPT-induced Chk2 autophosphorylation. Indeed, a concentration as low as 1 μM PV1019 was able to inhibit the TPT-induced Chk2 autophosphorylation (IC_{50} was 2.8 μM) (Fig. 3C).

It has been reported that in response to DNA damage, Chk2 phosphorylates HDMX on Ser^{367}, which leads to HDMX degradation (Fig. 3A). This degradation can be abrogated by the Chk2 inhibitor, ABI (Pereg et al., 2006). Figure 3E shows that exposure of MCF7 cells to 1 μM TPT for 4 h led to an expected decrease in the cellular level of HDMX. Coincubating the cells with PV1019 decreased the level of HDMX degradation induced by TPT exposure. Abrogation of HDMX degradation after TPT treatment by PV1019 provides evidence of PV1019 inhibiting Chk2 activity.

We also observed that the level of IR-induced Ser^{516} phosphorylation was significantly decreased when MCF7 cells were exposed to PV1019 at 10 or 25 μM (IC_{50} <10 μM) (Fig. 3F). Likewise, under identical assay conditions, the level of IR-induced Cdc25C phosphorylation on Ser^{216} was decreased by more than 50% in the presence of 10 μM PV1019. These data provide convergent evidence for cellular inhibition of Chk2 by PV1019.

Abrogation of IR-Induced Apoptosis in Mouse Thymocytes by PV1019. Chk2 activation is known to induce apoptosis in thymocytes by activating p53 (Hirao et al., 2000). To further investigate the inhibitory effect of PV1019 on Chk2, we studied IR-induced apoptosis in normal mouse thymocytes. In a previous study, *Chk2*(−/−) mouse thymocytes were shown to be resistant to IR (Hirao et al., 2000). In addition, the recently reported Chk2 inhibitor VRX0466617 was shown to abrogate IR-induced apoptosis in normal mouse thymocytes (Carlessi et al., 2007). We performed experiments with PV1019 to test whether we could emulate this phenomenon using flow cytometry to measure sub-G_1 (apoptotic) cells. Figure 4A shows the effect of 5 Gy of IR on wild-type mouse thymocytes. IR exposure produced a large sub-G_1 fraction of cells (71.9%) compared with untreated control cells (11.5%). Pretreatment of normal thymocytes with PV1019 showed a decrease in the sub-G_1 fraction (56%). Furthermore, in *Chk2*(−/−) cells, exposure to 5 Gy of IR and incubation for 16 h showed a comparable reduction of the sub-G_1 cells from 71.9% (control thymocytes) to 52.2% [*Chk2*(−/−) thymocytes] (Fig. 4B). This result corroborates

TABLE 1

Kinase profiling data for PV1019

Experiments were performed by Reaction Biology Corp. (http://www.reactionbiology.com/) using a radioactive assay method. Ten concentration curves were run with 10 μM ATP. Kinases showing some inhibition are in bold, and evolutionarily related kinases (Manning et al., 2002) are in *italic*.

Kinase	PV1019 IC_{50}	Kinase	PV1019 IC_{50}
	nM		*nM*
ABL1	>20,000	IR	>20,000
ALK	>20,000	IRAK4	>20,000
AKT1 (dPH, S473D)	**10,900**	JAK2	>20,000
Aurora A	>20,000	JAK3	>20,000
BTK	>20,000	KDR/VEGFR2	>20,000
CAMKIIb	>20,000	LCK	>20,000
CDK1/cyclinB	**1,835**	Lyn	>20,000
CDK2/cyclinA	>20,000	**MINK**	**2,261**
Chk1	*15,730*	MST2/STK3	>20,000
Chk2	*24*	P38α/MAPK14	>20,000
c-MET	>20,000	**PAK2**	**8,579**
c-Src	>20,000	PDGFRa	>20,000
DAPK1	*8,743*	*PHKg2*	**5,707**
EGFR	>20,000	*PIM1*	**4,749**
EphA3	>20,000	**PKA**	**9,469**
EphB4	>20,000	PKCα	>20,000
ErbB4/HER4	>20,000	PLK2	>20,000
ERK1	>20,000	RET	>20,000
ERK2/MAPK2/P42MAPK	>20,000	**ROCK-I**	**9,405**
FGFR1	>20,000	**RSK1**	**10,970**
FGFR2	>20,000	**RSK2**	**3,613**
FGFR3	>20,000	Syk	>20,000
FLT1/VEGFR1	>20,000	TAK1-TAB1	>20,000
FLT3	>20,000	TIE2	>20,000
FLT4	>20,000	TRKA/NTRK1	>20,000
GSK3β	>20,000	ZAP70	>20,000
HIPK1	**10,780**		

ALK, anaplastic lymphoma kinase; BTK, Bruton's tyrosine kinase; CAMK, Ca^{2+}/calmodulin-dependent protein kinase; CDK, cyclin-dependent kinase; CHK, C-terminal Src kinase-homologous kinase; DAPK, death-associated protein kinase; EGFR, epidermal growth factor receptor; Eph, ephrin type A receptor; ERK, extracellular signal-regulated kinase; MAPK, mitogen-activated protein kinase; FGFR, fibroblast growth factor receptor; VEGFR, vascular endothelial growth factor receptor; FLT, FMS-like tyrosine kinase; GSK, glycogen synthase kinase; HIPK, homeodomain interacting protein kinase; IRAK, interleukin-1 receptor-associated kinase; JAK, Janus tyrosine kinase; KDR, kinase insert domain receptor; LCK, lymphocyte-specific protein tryosine kinase; MINK, Misshapen/NIKs-related kinase; MST, mammalian STE20-like kinase; STK, serine/threonine kinase 3; PAK, p21-activated kinase; PDGFR, platelet-derived growth factor receptor; PHKg2, phosphorylase kinase γ2 ; PK, protein kinase; PLK, polo-like kinase; ROCK, Rho-associated kinase; RSK, ribosomal S6 kinase; Syk, spleen tyrosine kinase; TAK, transforming growth factor-β -activated kinase; TAB, transforming growth factor-β-activated protein kinase-binding protein; NTRK, neurotrophic tyrosine kinase receptor; ZAP70, ζ -chain-associated protein kinase 70.

the observed effect of PV1019 decreasing the number of sub-G_1 cells in Chk2 wild-type cells after exposure to IR (Fig. 4A). These data provide further evidence for the inhibition of cellular Chk2 by PV1019.

PV1019 Potentiates the Activity of Chemotherapeutic Agents in Human Tumor Cells. To test whether Chk2 inhibition could sensitize the cells to chemotherapeutic agents, we investigated whether PV1019 could enhance the effect of topoisomerase I inhibitors and ionizing radiation in human tumor cells. We used two different ovarian cancer cell lines from the NCI-60 cell panel to evaluate the effect of PV1019. Figure 5A shows that concentrations of 3 and 25 μM PV1019 augmented the growth inhibitory effect of TPT, decreasing the IC_{50} up to 5.7-fold (25 μM PV1019) in OVCAR-5 after a 48-h exposure period. The IC_{50} of PV1019 alone was 58 μM. To confirm that PV1019 synergized the effect of TPT, we calculated combination indices with a range of concentrations of PV1019 and TPT using the program CalcuSyn. Figure 5B shows synergy because the combination indices were below 1 (Chou and Talalay, 1984). We also examined the effect of the combination of PV1019 and TPT in OVCAR-4 cells (Fig. 5C). A full growth inhibitory response was not achieved with increasing concentrations of TPT alone, although an IC_{50} was attained. However, PV1019 increased the maximum growth inhibitory effect of TPT, whereas the IC_{50} of PV1019 alone was 18.7 μM. Combination indices were calculated using CalcuSyn, and the values are tabulated in Fig. 5D. Again, synergism was observed in the OVCAR-4 cells. We also tested whether the growth inhibitory effect of the parental compound camptothecin (CPT) could also be augmented. Figure 5E shows that in OVCAR-4, PV1019 was able to enhance the maximum growth inhibitory of CPT, similar to TPT.

We next determined the effects of PV1019 on tumor cell (U251 cells) radiosensitivity. PV1019 at 5 μM provided approximately 33% toxicity with a 3-h incubation in U251 cells as a single agent. Treatment of U251 cells with 5 μM PV1019 (1 h before and 2 h after IR) radiosensitized U251 cells with a dose enhancement factor of 1.4 (Fig. 5F). Under these conditions the cell cycle profile of PV1019 did not change (data not shown).

Taken together, these results demonstrate that PV1019 potentiates the cell-killing effect of topoisomerase I inhibitors (TPT and CPT) and IR in several cancer cell lines.

Effect of Chk2 Inhibition or Down-Regulation of Chk2 on Growth of Tumor Cell Lines. It has been reported previously that HCT15 cells are functionally deficient for Chk2 because they express a mutant form of Chk2 that is rapidly degraded (Falck et al., 2001). To further investigate the selectivity of PV1019 for Chk2, we investigated the sensitivity of HCT15 cells to PV1019. Because HCT15 cells are part of the panel of colon carcinoma cell lines in the NCI-60 cell panel (http://discover.nci.nih.gov/cellminer/), we compared the antiproliferative activity of PV1019 across the colon and ovarian cell lines from the NCI-60 cell panel. Figure 6, A and B, show growth inhibitory responses. HCT15 cells,

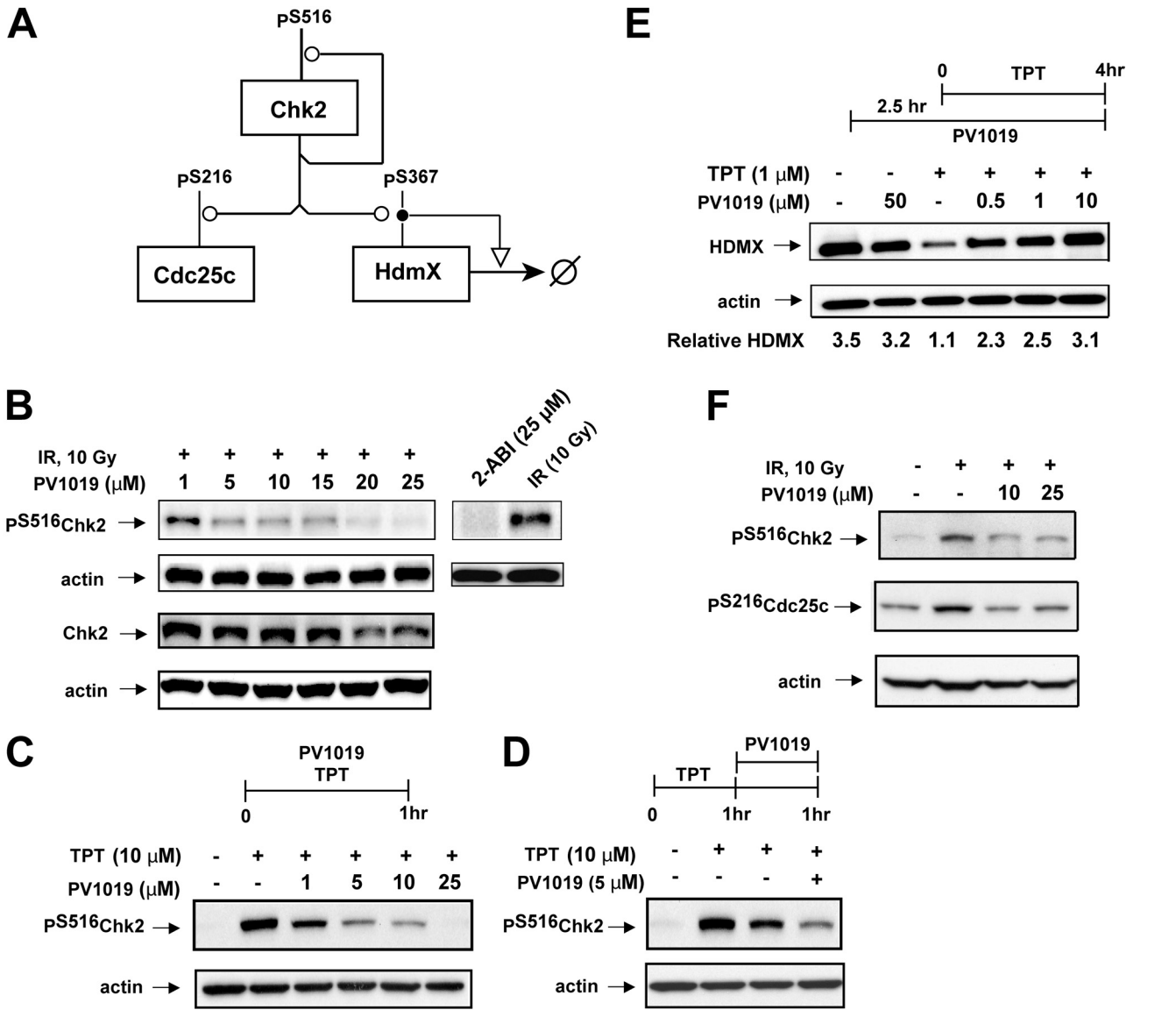

Fig. 3. Evidence for cellular inhibition of Chk2 by PV1019. A, abbreviated molecular interaction map depicting the phosphorylations of Chk2, Cdc25C, and HDMX after Chk2 activation. The conventions used for the interactions (Kohn, 1999) are as follows: the line with an open circle indicates enzymatic stimulation and phosphorylation, the line with an open arrowhead indicates general stimulation, and the open circle with a line crossing through indicates degradation. For details of the molecular interaction map for Chk2 see Pommier et al. (2006). B, OVCAR-4 cells were exposed to 10 Gy of IR followed by a 1-h incubation in the presence or absence of PV1019 or ABI (preincubated for 1 h). The levels of Chk2 phosphorylated on Ser^{516} and total Chk2 were detected by Western blotting. Actin was used as a loading control. C, OVCAR-5 cells were exposed to PV1019 and TPT (or control) for 1 h. The levels of Chk2 phosphorylated on Ser^{516} were detected by Western blotting. Actin was used as a loading control. D, OVCAR-5 cells were pretreated with TPT for 1 h, the drug was washed off, and the cells were exposed to PV1019 (or control) for an additional hour. The levels of Chk2 phosphorylated on Ser^{516} were detected by Western blotting. Actin was used as loading control. E, MCF7 cells were exposed to either 1 μM TPT for 4 h or 10 Gy of IR followed by a 4-h incubation in the presence or absence of PV1019 (preincubated for 2.5 h). Western blotting using anti-HDMX antibodies was performed to measure the levels of HDMX. Representative gels are depicted, and the quantified levels of HDMX are shown in the graphs. F, MCF7 cells were exposed to 10 Gy of IR followed by a 1-h incubation in the presence or absence of PV1019 (preincubated for 2.5 h). The levels of Chk2 phosphorylated on Ser^{516} were detected by Western blotting (top panel). The levels of Cdc25C phosphorylated on Ser^{516} were detected by Western blotting (bottom panel). Actin was used as a loading control for each experiment.

which are known to be deficient for Chk2 (Fig. 6C), showed resistance to PV1019 compared with the other colon cell lines. In addition, we observed that SK-OV3 cells also showed a lack of PV1019-mediated growth inhibition. Western blotting showed almost undetectable levels of Chk2 in SK-OV3 (Fig. 6D). In contrast, KM12, OVCAR-3, OVCAR-4, and OVCAR-8 cells, which were among the most sensitive to PV1019 (Fig. 6, A and B), expressed high levels of Chk2 (Fig. 6, C and D). These data are consistent with the possibility that the antiproliferative effects mediated by PV1019 are related to Chk2 inhibition.

To confirm the antiproliferative effect of Chk2 inhibition in human tumor cells, we investigated the effect of RNAi-mediated gene silencing of *CHEK2* in two different ovarian cell lines, OVCAR-4 and OVCAR-8, that express high levels of Chk2 (Fig. 6, C and D). The *CHEK2* RNAi used has been previously validated and reported (Zhang et al., 2009). In both cell lines down-regulation of *CHEK2* caused a growth inhibitory effect compared with the RNAi control (Fig. 6, E and F). An additional *CHEK2* siRNA was also used in OVCAR-8 cells and showed a similar inhibitory effect (data not shown). These data provide evidence that Chk2 inhibi-

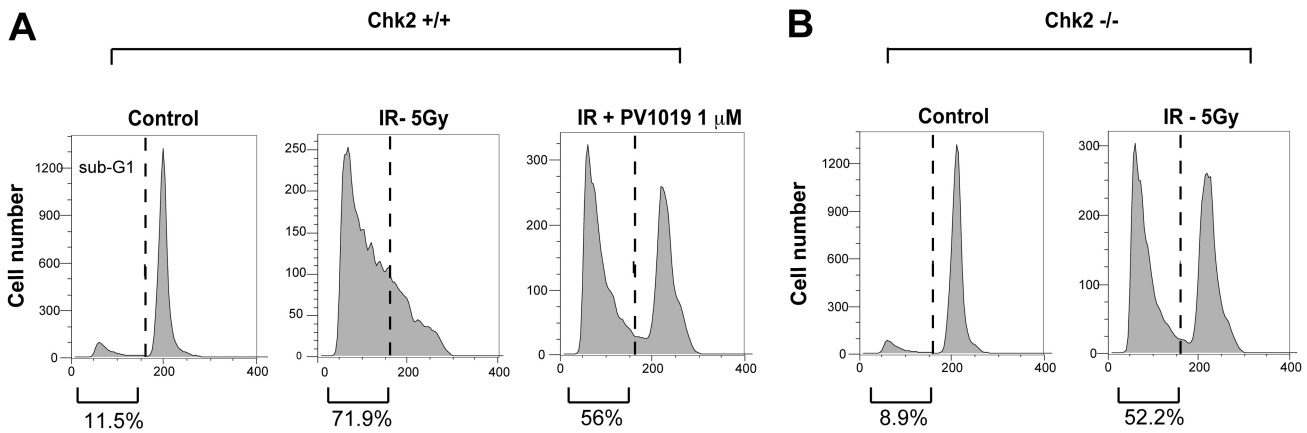

Fig. 4. Abrogation of IR-induced apoptosis by PV1019 in mouse thymocytes. Wild-type (A) or *Chk2*(−/−) (B) mouse thymocytes were isolated and exposed to 5 Gy IR (or control) and incubated for 16 h in the presence or absence of 1 μM PV1019 (preincubated for 1 h). Cells were stained with propidium iodide and analyzed by flow cytometry. Representative graphs show the number of cells in G_1 and sub-G_1 cell cycle phases. The percentage of cells in either the G_1 or sub-G_1cell cycle phase is shown.

tion can produce antiproliferative activity in cancer cells that express high endogenous Chk2 levels.

Discussion

We recently identified and characterized a Chk2 inhibitor, NSC 109555, with a novel chemotype (Jobson et al., 2007) and cocrystallized NSC 109555 with the catalytic domain of Chk2 (Lountos et al., 2009). Seeking to improve the cellular activity of NSC 109555 while maintaining selectivity for Chk2, we synthesized a new analog PV1019 (NSC 744039) (Fig. 1A). In the present study, we report that PV1019 is an ATP-competitive inhibitor (Fig. 1D) that exhibits cellular Chk2 inhibition while exhibiting higher potency than NSC 109555 and retaining specificity for Chk2 (IC_{50} of 24–260 nM) (Fig. 1; Table 1).

Because the IC_{50} values determined in the in vitro kinase assays and cellular assays (Figs. 1 and 3, respectively) showed an approximately 100-fold difference, we examined the activity of PV1019 in the presence of physiological concentrations of ATP to better relate the relationship between in vitro kinase and cellular inhibition results. As expected, a more physiological concentration of ATP (1 mM) decreased the activity of PV1019, which may explain the higher (low micromolar) concentration required to inhibit Chk2 in cells. In addition, we cannot exclude the impact of drug uptake and any metabolism/degradation of PV1019 in the cellular studies.

Selectivity for Chk2 was maintained with PV1019 as demonstrated via a kinase panel profiling experiment. Importantly, as with NSC 109555, PV1019 was markedly more selective for Chk2 than for Chk1 (655-fold) (Table 1). Other agents that are under clinical evaluation do not elicit this specificity for Chk2 over Chk1. Thus, PV1019 may provide a novel chemotype for developing new therapeutic agents. A number of the kinases that showed some inhibition by PV1019 (death-associated protein kinase 1, Chk1, phosphorylase kinase γ2, PIM1, ribosomal S6 kinase 1, and ribosomal S6 kinase 2) (shown in italics in Table 1) are part of the same phylogenic tree in the human kinome, Ca^{2+}/calmodulin-dependent protein kinase (Manning et al., 2002). This observation demonstrates the potential difficulty of developing highly specific kinase inhibitors. However, in the case of PV1019, at least a 75-fold selectivity was observed for Chk2 over the other kinases tested.

In this study, we have demonstrated that PV1019 is capable of inhibiting the kinase activity of Chk2 in a cellular environment. We have shown inhibition of Chk2 and abrogation of downstream substrate phosphorylation/function for Cdc25C and HDMX by PV1019 (Fig. 3, B, C, and D). In addition, the level of Chk2-dependent IR-induced apoptosis was decreased by PV1019 in normal mouse thymocytes (Fig. 4A), which is in accordance with another Chk2 inhibitor, VRX0466617 (Carlessi et al., 2007). Taken together, these cellular assays demonstrate inhibition of Chk2 activity by PV1019 in cells. We also found a correlation between the antiproliferative activity of PV1019 in the ovarian and colon cell lines from the NCI-60 cell screen from the Developmental Therapeutics Program and the levels of Chk2 expression.

Chk2 inhibitors have been proposed as chemotherapeutic agents in combination with cytotoxic agents [for review, see Pommier et al. (2005) and Antoni et al. (2007)]. This hypothesis has not been clearly demonstrated when pharmacological inhibition of Chk2 is combined with cytotoxic agents. Indeed, a recently reported Chk2 inhibitor, VRX0466617, did not show synergy with a number of anticancer agents (Carlessi et al., 2007). However, the authors could not exclude the possibility that VRX0466617 inhibits Aurora A kinase. In our studies we used OVCAR-4 and OVCAR-5 ovarian human tumor cells to test this hypothesis with cytotoxic agents. We have demonstrated synergy of cytotoxic agents in combination with PV1019 in those cell lines. Likewise, PV1019 was shown to enhance the cell killing of radiation in the human brain tumor cell line, U251. Taken together, our data suggest the use of a Chk2 inhibitor in combination with topoisomerase I inhibitor chemotherapy or radiation. In addition to the use of Chk2 inhibitors with either cytotoxic agents or radiation, we have also shown the potential of using PV1019 as a single agent. Indeed, down-regulation of Chk2 leads to growth inhibition in two of the ovarian cell lines with the highest Chk2 expression, AVCAR4 and OVCAR8, whereas the two Chk2-deficient cell lines, HCT15 (Falck et al., 2001) and SK-OV3, are not affected by PV1019 (Fig. 6). These results suggest the potential activity of Chk2 inhibitors as single agents in cancer cells with high Chk2 expression.

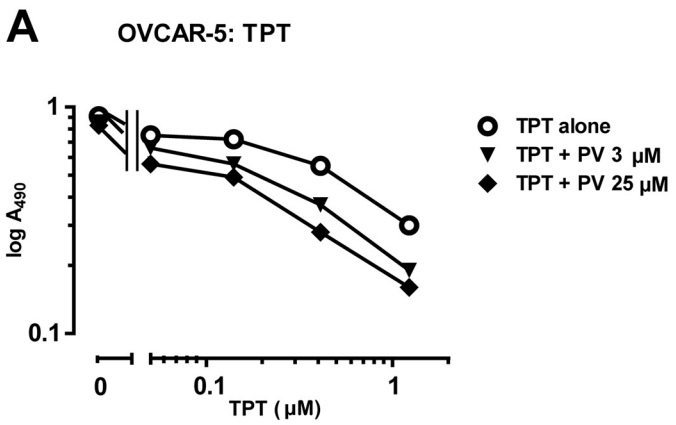

B

Combination Index (CI) values for PV1019 and TPT in OVCAR-5 cells

PV1019 μM	TPT μM 0.1	0.4	1.2
3	0.56	0.45	0.32
6	0.75	0.59	0.38
12.5	0.80	0.69	0.44
25	0.77	0.52	0.43

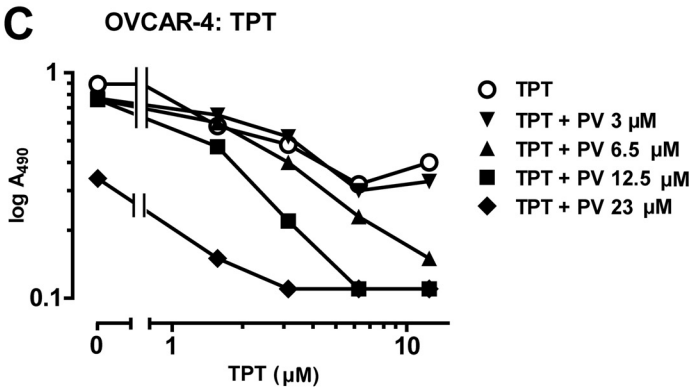

D

Combination Index (CI) values for PV1019 and TPT in OVCAR-4 cells

PV1019 μM	TPT μM 3.1	6.3	12.5
12.5	0.50	0.34	0.48
23	0.45	0.50	0.43

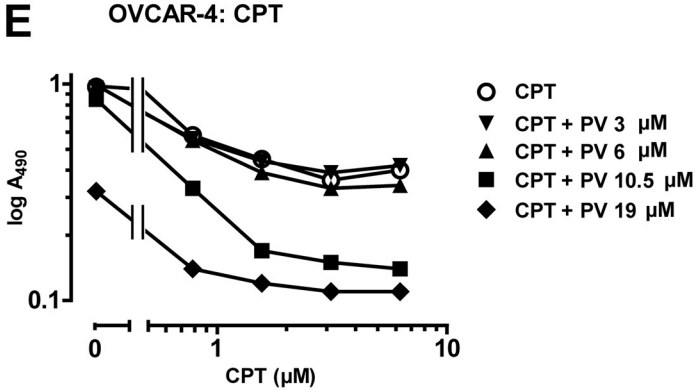

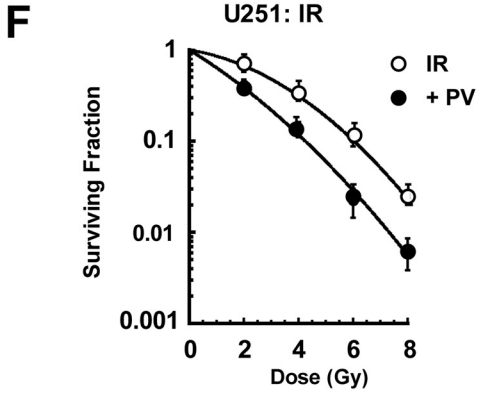

Fig. 5. PV1019 (PV) synergistically inhibits cellular proliferation with topoisomerase I inhibitors in ovarian human tumor cell lines and synergizes the effect of radiation in the brain tumor cell line, U251. Cells from the indicated cell lines OVCAR-5 (A) and OVCAR-4 (C and E) were incubated with various concentrations of TPT (A and C) and CPT (E) alone or coincubated with various concentrations of TPT or CPT and fixed concentrations of PV1019 for 48 h in 96-well plates. MTS was added to the plates and the absorbance at 495 nm was measured. Combination indices for A and C were calculated using CalcuSyn software, and the values were tabulated (B and D, respectively). F, U251 cells were seeded in six-well tissue culture plates, and radiation was delivered 16 h later. U251 cells were treated with 5 μM PV1019 1 h before different dose (0, 2, 4, 6, and 8 Gy) of IR. All cells including DMSO vehicle control were rinsed with PBS, and cultures were replaced with fresh growth medium 2 h after IR. The number of colonies was determined 10 days later, and survival curves were generated after normalizing for cell killing by PV1019 alone. Dose enhancement factor was calculated at a surviving fraction of 0.1. The average plating efficiency with 5 μM PV1019 alone was approximately 67%. Data represent the mean ± S.E. from four independent experiments in triplicate.

Determination of the crystal structure of the catalytic domain of Chk2 in complex with PV1019 provided a detailed view of the molecular interactions between the compound and the ATP-binding pocket and enabled us to compare and contrast its mode of binding with that of the lead compound NSC 109555 (Fig. 2D). PV1019 retains many of the same interactions with the ATP-binding pocket that were observed in the complex with NSC 109555 (Lountos et al., 2009), including the hydrogen bond with Glu^{273} and the hydrophobic interactions between the aryl and methyl moieties of the phenyl guanidinohydrazone and the ATP-binding pocket. The methyl group of PV1019 also projects toward a hydrophobic pocket in the enzyme as observed previously in the Chk2/NSC 109555 complex. This hydrophobic pocket is of considerable interest because it may present an opportunity to modulate the potency and specificity of Chk2 inhibitors; its shape, accessibility, and degree of hydrophobicity vary among kinases (Toledo et al., 1999; Scapin, 2002; Lountos et al., 2009). Accordingly, functional replacements for the methyl group of PV1019, such as branched and cyclic al-

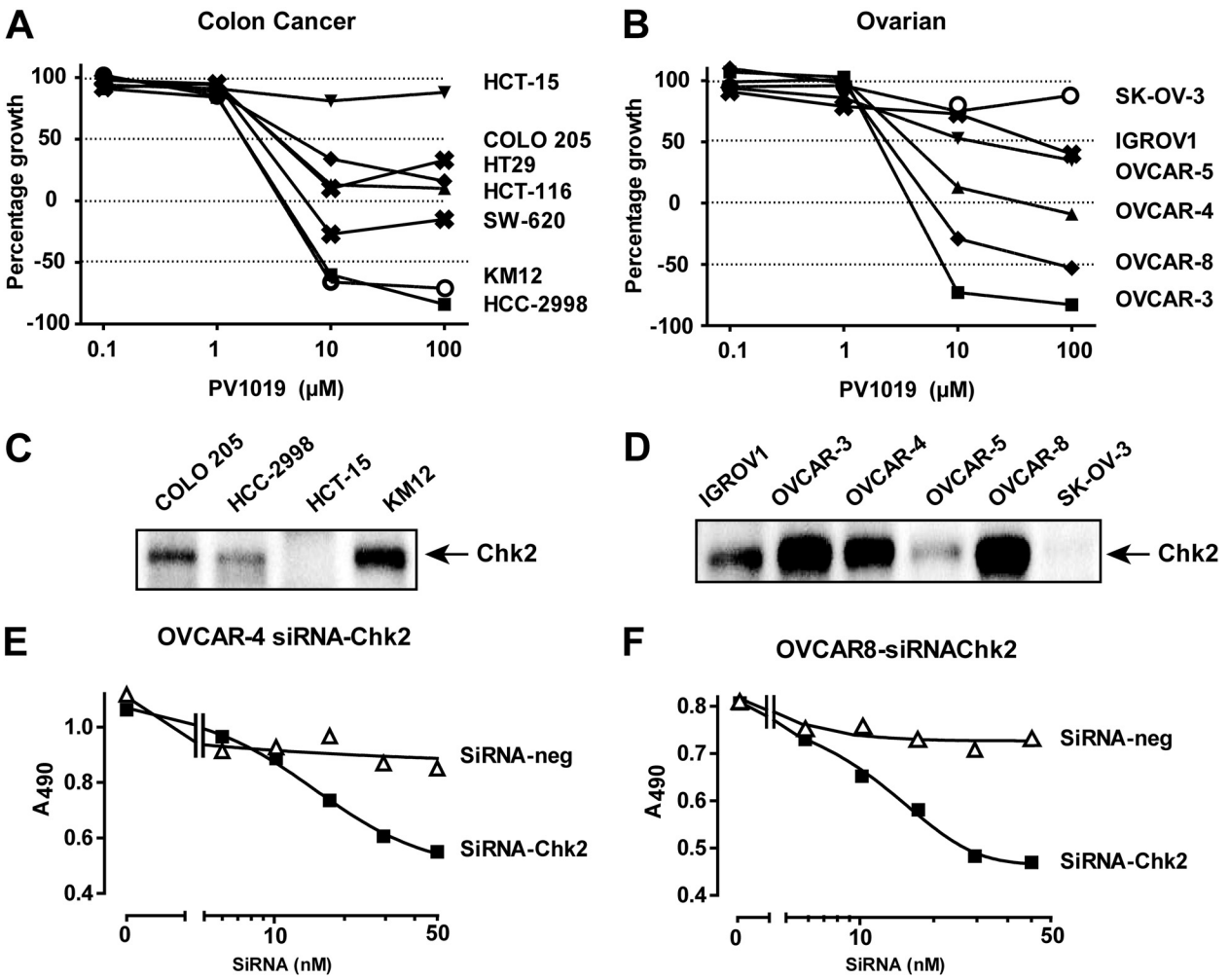

Fig. 6. PV1019 causes growth inhibition in a panel of colon and ovarian human tumor cell lines that mimics the effect of Chk2 RNAi in ovarian human tumor cells. A, the human colon carcinoma cell lines from the NCI-60 were incubated with varying concentrations of PV1019 for 48 h. The cells were subjected to the sulforhodamine assay and GI_{50} values were determined. B, the human tumor ovarian cell lines from the NCI-60 were incubated with varying concentrations of PV1019 for 48 h. The cells were subjected to the sulforhodamine B assay and GI_{50} values were determined. C and D, Chk2 protein levels measured by Western blot in the colon (C) and ovarian (D) cell lines from the National Cancer Institute Developmental Therapeutics Program screen. E, OVCAR-4 cells were transfected with either control siRNA or *CHEK2* siRNA and incubated for 96 h in 96-well plates. MTS was added to the plates and the absorbance at 495 nm was measured. Representative experiments are shown. F, OVCAR-8 cells were transfected with either control siRNA or *CHEK2* siRNA and incubated for 96 h in 96-well plates. MTS was added to the plates, and the absorbance at 495 nm was measured. Representative experiments are shown.

kanes, may fill this pocket and further improve potency and specificity. Because of the incorporation of the 7-nitroindole substituent, PV1019 picks up new interactions with the ATP-binding pocket, which probably account for its increased potency over the parent compound NSC 109555 (Lountos et al., 2009). The 7-nitro group incorporates two new interactions, a water-mediated hydrogen bond to the backbone carbonyl oxygen of Glu^{302} and a hydrogen bond to the backbone amide of Met^{304} in the hinge, and the amide nitrogen of PV1019 also picks up a water-mediated hydrogen bond to the carboxyl side chain oxygen of Glu^{308}. The indole ring is also involved in favorable van der Waals interactions with several hydrophobic residues in the ATP-binding pocket. Taken together, the conservation of the molecular interactions with the phenyl guanidinohydrazone and the new molecular interactions with the 7-nitroindole group probably contribute to the increased potency of PV1019. These observations will facilitate the further development of PV1019 derivatives.

In summary, we have developed a potent and specific inhibitor of Chk2. We have shown inhibition in a cellular context and demonstrated that the inhibitor synergizes two cytotoxic agents and radiation in human tumor cell lines and can by itself inhibit the growth of Chk2-overexpressing cells. These data provide evidence to consider this inhibitor for preclinical development in animal models.

Acknowledgments

We thank Dr. Noboru (National Center for Geriatrics and Ontology, Aichi, Japan) and Dr. Liu Cao (National Heart, Lung, and Blood Institute, National Institutes of Health) for providing and isolating wild-type and *Chk2*(−/−) thymocytes. QIAGEN supplied the *CHEK2* siRNA used in this study to the National Cancer Institute as part of a Collaborative Research Agreement. We thank Tamara Jones for technical assistance.

References

Ahn J and Prives C (2002) Checkpoint kinase 2 (Chk2) monomers or dimers phosphorylate Cdc25C after DNA damage regardless of threonine 68 phosphorylation. *J Biol Chem* **277:**48418–48426.

Ahn JY, Schwarz JK, Piwnica-Worms H, and Canman CE (2000) Threonine 68

phosphorylation by ataxia telangiectasia mutated is required for efficient activation of Chk2 in response to ionizing radiation. *Cancer Res* **60:**5934–5936.
Antoni L, Sodha N, Collins I, and Garrett MD (2007) CHK2 kinase: cancer susceptibility and cancer therapy—two sides of the same coin? *Nat Rev Cancer* **7:**925–936.
Arienti KL, Brunmark A, Axe FU, McClure K, Lee A, Blevitt J, Neff DK, Huang L, Crawford S, Pandit CR, et al. (2005) Checkpoint kinase inhibitors: SAR and radioprotective properties of a series of 2-arylbenzimidazoles. *J Med Chem* **48:**1873–1885.
Ariumi Y, Kuroki M, Dansako H, Abe K, Ikeda M, Wakita T, and Kato N (2008) The DNA damage sensors ataxia-telangiectasia mutated kinase and checkpoint kinase 2 are required for hepatitis C virus RNA replication. *J Virol* **82:**9639–9646.
Ashwell S, Janetka JW, and Zabludoff S (2008) Keeping checkpoint kinases in line: new selective inhibitors in clinical trials. *Expert Opin Investig Drugs* **17:**1331–1340.
Bartkova J, Horejsí Z, Koed K, Krämer A, Tort F, Zieger K, Guldberg P, Sehested M, Nesland JM, Lukas C, et al. (2005) DNA damage response as a candidate anti-cancer barrier in early human tumorigenesis. *Nature* **434:**864–870.
Carlessi L, Buscemi G, Larson G, Hong Z, Wu JZ, and Delia D (2007) Biochemical and cellular characterization of VRX0466617, a novel and selective inhibitor for the checkpoint kinase Chk2. *Mol Cancer Ther* **6:**935–944.
Castedo M, Perfettini JL, Roumier T, Yakushijin K, Horne D, Medema R, and Kroemer G (2004) The cell cycle checkpoint kinase Chk2 is a negative regulator of mitotic catastrophe. *Oncogene* **23:**4353–4361.
Chabalier-Taste C, Racca C, Dozier C, and Larminat F (2008) BRCA1 is regulated by Chk2 in response to spindle damage. *Biochim Biophys Acta* **1783:**2223–2233.
Chou TC and Talalay P (1984) Quantitative analysis of dose-effect relationships: the combined effects of multiple drugs or enzyme inhibitors. *Adv Enzyme Regul* **22:**27–55.
Curman D, Cinel B, Williams DE, Rundle N, Block WD, Goodarzi AA, Hutchins JR, Clarke PR, Zhou BB, Lees-Miller SP, et al. (2001) Inhibition of the G_2 DNA damage checkpoint and of protein kinases Chk1 and Chk2 by the marine sponge alkaloid debromohymenialdisine. *J Biol Chem* **276:**17914–17919.
Falck J, Lukas C, Protopopova M, Lukas J, Selivanova G, and Bartek J (2001) Functional impact of concomitant versus alternative defects in the Chk2–p53 tumour suppressor pathway. *Oncogene* **20:**5503–5510.
Ghosh JC, Dohi T, Raskett CM, Kowalik TF, and Altieri DC (2006) Activated checkpoint kinase 2 provides a survival signal for tumor cells. *Cancer Res* **66:**11576–11579.
Gorgoulis VG, Vassiliou LV, Karakaidos P, Zacharatos P, Kotsinas A, Liloglou T, Venere M, Ditullio RA Jr, Kastrinakis NG, Levy B, et al. (2005) Activation of the DNA damage checkpoint and genomic instability in human precancerous lesions. *Nature* **434:**907–913.
Hirao A, Kong YY, Matsuoka S, Wakeham A, Ruland J, Yoshida H, Liu D, Elledge SJ, and Mak TW (2000) DNA damage-induced activation of p53 by the checkpoint kinase Chk2. *Science* **287:**1824–1827.
Jobson AG, Cardellina JH 2nd, Scudiero D, Kondapaka S, Zhang H, Kim H, Shoemaker R, and Pommier Y (2007) Identification of a bis-guanylhydrazone [4,4′-diacetyldiphenylurea-bis(guanylhydrazone); NSC 109555] as a novel chemotype for inhibition of Chk2 kinase. *Mol Pharmacol* **72:**876–884.
Kohn KW (1999) Molecular interaction map of the mammalian cell cycle control and DNA repair systems. *Mol Biol Cell* **10:**2703–2734.
Lapenna S and Giordano A (2009) Cell cycle kinases as therapeutic targets for cancer. *Nat Rev Drug Discov* **8:**547–566.
Larson G, Yan S, Chen H, Rong F, Hong Z, and Wu JZ (2007) Identification of novel, selective and potent Chk2 inhibitors. *Bioorg Med Chem Lett* **17:**172–175.
Lau A, Swinbank KM, Ahmed PS, Taylor DL, Jackson SP, Smith GC, and O'Connor MJ (2005) Suppression of HIV-1 infection by a small molecule inhibitor of the ATM kinase. *Nat Cell Biol* **7:**493–500.
Lountos GT, Tropea JE, Zhang D, Jobson AG, Pommier Y, Shoemaker RH, and Waugh DS (2009) Crystal structure of checkpoint kinase 2 in complex with NSC 109555, a potent and selective inhibitor. *Protein Sci* **18:**92–100.
Manning G, Whyte DB, Martinez R, Hunter T, and Sudarsanam S (2002) The protein kinase complement of the human genome. *Science* **298:**1912–1934.
Matsuoka S, Huang M, and Elledge SJ (1998) Linkage of ATM to cell cycle regulation by the Chk2 protein kinase. *Science* **282:**1893–1897.
Matthews DJ, Yakes FM, Chen J, Tadano M, Bornheim L, Clary DO, Tai A, Wagner JM, Miller N, Kim YD, et al. (2007) Pharmacological abrogation of S-phase checkpoint enhances the anti-tumor activity of gemcitabine in vivo. *Cell Cycle* **6:**104–110.
Oliver AW, Paul A, Boxall KJ, Barrie SE, Aherne GW, Garrett MD, Mittnacht S, and Pearl LH (2006) Trans-activation of the DNA-damage signalling protein kinase Chk2 by T-loop exchange. *EMBO J* **25:**3179–3190.
Pereg Y, Lam S, Teunisse A, Biton S, Meulmeester E, Mittelman L, Buscemi G, Okamoto K, Taya Y, Shiloh Y, et al. (2006) Differential roles of ATM- and Chk2-mediated phosphorylations of Hdmx in response to DNA damage. *Mol Cell Biol* **26:**6819–6831.
Pommier Y, Sordet O, Rao VA, Zhang H, and Kohn KW (2005) Targeting chk2 kinase: molecular interaction maps and therapeutic rationale. *Curr Pharm Des* **11:**2855–2872.
Pommier Y, Weinstein JN, Aladjem MI, and Kohn KW (2006) Chk2 molecular interaction map and rationale for Chk2 inhibitors. *Clin Cancer Res* **12:**2657–2661.
Scapin G (2002) Structural biology in drug design: selective protein kinase inhibitors. *Drug Discov Today* **7:**601–611.
Sharma V and Tepe JJ (2004) Potent inhibition of checkpoint kinase activity by a hymenialdisine-derived indoloazepine. *Bioorg Med Chem Lett* **14:**4319–4321.
Solier S, Sordet O, Kohn KW, and Pommier Y (2009) Death receptor-induced activation of the Chk2- and histone H2AX-associated DNA damage response pathways. *Mol Cell Biol* **29:**68–82.
Takai H, Naka K, Okada Y, Watanabe M, Harada N, Saito S, Anderson CW, Appella E, Nakanishi M, Suzuki H, et al. (2002) Chk2-deficient mice exhibit radioresistance and defective p53-mediated transcription. *EMBO J* **21:**5195–5205.
Toledo LM, Lydon NB, and Elbaum D (1999) The structure-based design of ATP-site directed protein kinase inhibitors. *Curr Med Chem* **6:**775–805.
Vakifahmetoglu H, Olsson M, Tamm C, Heidari N, Orrenius S, and Zhivotovsky B (2008) DNA damage induces two distinct modes of cell death in ovarian carcinomas. *Cell Death Differ* **15:**555–566.
Wu X and Chen J (2003) Autophosphorylation of checkpoint kinase 2 at serine 516 is required for radiation-induced apoptosis. *J Biol Chem* **278:**36163–36168.
Yu Q, La Rose J, Zhang H, Takemura H, Kohn KW, and Pommier Y (2002) UCN-01 inhibits p53 up-regulation and abrogates γ-radiation-induced G_2-M checkpoint independently of p53 by targeting both of the checkpoint kinases, Chk2 and Chk1. *Cancer Res* **62:**5743–5748.
Yu Q, Rose JH, Zhang H, and Pommier Y (2001) Antisense inhibition of Chk2/hCds1 expression attenuates DNA damage-induced S and G_2 checkpoints and enhances apoptotic activity in HEK-293 cells. *FEBS Lett* **505:**7–12.
Zabludoff SD, Deng C, Grondine MR, Sheehy AM, Ashwell S, Caleb BL, Green S, Haye HR, Horn CL, Janetka JW, et al. (2008) AZD7762, a novel checkpoint kinase inhibitor, drives checkpoint abrogation and potentiates DNA-targeted therapies. *Mol Cancer Ther* **7:**2955–2966.
Zhang YW, Jones TL, Martin SE, Caplen NJ, and Pommier Y (2009) Implication of checkpoint kinase-dependent up-regulation of ribonucleotide reductase R2 in DNA damage response. *J Biol Chem* **284:**18085–18095.

Address correspondence to: Dr. Yves Pommier, Chief, Laboratory of Molecular Pharmacology, Center for Cancer Research, National Cancer Institute, NIH, Bethesda, MD 20892-4255. E-mail: pommier@nih.gov